



Overexpression of acid ceramidase (ASAH1) protects retinal cells (ARPE19) from oxidative stress[§]

Eriko Sugano,^{1,*} Genea Edwards,^{2,†} Saikat Saha,^{2,†} Lynda A. Wilmott,^{2,†} Richard C. Grambergs,^{2,†} Koushik Mondal,^{2,†} Hui Qi,[§] Megan Stiles,[§] Hiroshi Tomita,^{1,*} and Nawajes Mandal^{3,†,§,*}

Division of Science and Engineering,* Iwate University, Morioka 020-8551, Japan; Departments of Ophthalmology[†] and Anatomy and Neurobiology,** University of Tennessee Health Science Center, Memphis, TN 38163; and Department of Ophthalmology,[§] University of Oklahoma Health Science Center, Oklahoma City, OK 73104

Abstract Over 11 million people in the United States alone have some form of age-related macular degeneration (AMD). Oxidative stress, cell death, and the degeneration of retinal pigment epithelial (RPE) cells contribute to AMD pathology. Recent evidence suggests that ceramide (Cer), a cellular sphingolipid mediator that acts as a second messenger to induce apoptosis, might play a role in RPE cell death. The lysosomal breakdown of Cer by acid ceramidase [N-acylsphingosine amidohydrolase (ASAH)1] into sphingosine (Sph) is the major source for Sph 1-phosphate production, which has an opposing role to Cer and provides cytoprotection. Here, we investigated the role of Cer in human RPE-derived ARPE19 cells under hydrogen peroxide-induced oxidative stress, and show that Cer and hexosyl-Cer levels increase in the oxidatively stressed ARPE19 cells, which can be prevented by overexpression of lysosomal ASAH1. This study demonstrates that oxidative stress generates sphingolipid death mediators in retinal cells and that induction of ASAH1 could rescue retinal cells from oxidative stress by hydrolyzing excess Cers.—Sugano, E., G. Edwards, S. Saha, L. A. Wilmott, R. C. Grambergs, K. Mondal, H. Qi, M. Stiles, H. Tomita, and N. Mandal. Overexpression of acid ceramidase (ASAH1) protects retinal cells (ARPE19) from oxidative stress. *J. Lipid Res.* 2019. 60: 30–43.

Supplementary key words N-acylsphingosine amidohydrolase 1 • ceramide • hexosyl-ceramide • lysosome, retinal pigment epithelium • retinal degeneration • age-related macular degeneration

This work was supported by National Eye Institute Grants EY022071, EY025256, and EY021725, and grants from the Foundation Fighting Blindness and Research to Prevent Blindness. Additional support was provided by Ministry of Education, Culture, Sports, Science and Technology Grants-in-Aid for Scientific Research 16K11314, 16H05485, and 16K15729. The lipidomic services (Virginia Commonwealth University Lipidomics/Metabolomics Core) and products in support of the study were generated, in part, by the Virginia Commonwealth University Massey Cancer Center, with funding from National Institutes of Health Grant P30 CA016059. The content is solely the responsibility of the authors and does not necessarily represent the official views of the National Institutes of Health, the Department of Veterans Affairs, or the US Government.

Manuscript received 27 November 2017 and in revised form 26 October 2018.

Published, JLR Papers in Press, November 9, 2018

DOI <https://doi.org/10.1194/jlr.M082198>

Age-related macular degeneration (AMD) is the leading cause of blindness in the elderly population. More than 80% of AMD cases are of the dry-AMD classification, which characteristically features geographic atrophy resulting from the loss of retinal pigment epithelial (RPE) cells (1, 2). Dry-AMD often converts to wet-AMD, which is vision-threatening. Accumulation of undigested cellular debris (e.g., drusen), oxidative stress, and subsequent death and degeneration of RPE cells are important contributors to AMD pathology (3, 4). Accumulating evidence suggests that the cellular sphingolipid mediator, ceramide (Cer), which acts as a second messenger to induce apoptosis, might play a role in RPE cell death (5–7). Here, we investigate for the first time the role of Cer in human RPE-derived ARPE19 cells under oxidative stress by removing excess cellular Cer via genetic manipulation of Cer-hydrolyzing enzymes.

In addition to being a critical component of membrane structure and function, Cer serves as a vital intracellular second messenger. A steady-state level of Cer is necessary for cell proliferation and differentiation (8, 9), while excessive amounts of Cer are often toxic and can result in cellular apoptosis (10). High concentrations of Cer can result in the induction of cell death, leading to tissue damage and organ failure, such as what is observed in retinal degeneration

Abbreviations: AMD, age-related macular degeneration; ASAH, N-acylsphingosine amidohydrolase; BCL2, B-cell CLL/lymphoma 2, CCL2, C-C motif chemokine ligand 2; Cer, ceramide; CerS, ceramide synthase; cFOS, proto-oncogene C-Fos; dh-Sph, dihydro-sphingosine; HO-1, heme oxygenase (decycling) 1; Hex-Cer, hexosyl-ceramide; ICAM1, intercellular adhesion molecule 1; Lac-Cer, lactosyl-ceramide; LDH, lactate dehydrogenase; Ly-ARPE19, lysosomal ARPE19; PARP, poly (ADP-ribose) polymerase; RD, retinal degeneration; RPE, retinal pigment epithelial; SIP, sphingosine 1-phosphate; Sph, sphingosine; SPT2, serine palmitoyl transferase 2; Veh, vehicle.

¹E. Sugano and H. Tomita contributed equally to this work.

²G. Edwards, S. Saha, L. A. Wilmott, R. C. Grambergs, and K. Mondal contributed equally to this work.

³To whom correspondence should be addressed.

e-mail: nmandal@uthsc.edu

[§]The online version of this article (available at <http://www.jlr.org>) contains a supplement.

Copyright © 2019 by the American Society for Biochemistry and Molecular Biology, Inc.

This article is available online at <http://www.jlr.org>

(RD) (11, 12), systemic lupus erythematosus (13, 14), and diabetes mellitus (15). In contrast, a continuous basal level of Cer is essential in staving off many neurodegenerative diseases, such as Parkinson's disease (16–18) and Alzheimer's disease (18–21).

The generation of endogenous Cer is induced by noxious stimuli, such as UV A light (22) and proinflammatory cytokines (e.g., TNF- α) (23), both of which promote the release of Cer from SM and/or by the de novo synthesis pathway via palmitate (24). Cer induces apoptosis via multiple mechanisms, such as through the inhibition of AKT-1 and activation of extrinsic and intrinsic apoptotic pathways (15). These pathways converge on the cleavage of caspase-3 and result in DNA fragmentation, degradation of the cytoskeleton and nuclear proteins, and the formation of apoptotic bodies, including DNA fragments (e.g., DNA ladder) (25). Apoptotic cell death is the potential driver for retinal neuron degeneration (e.g., photoreceptor cells, ganglion cells, and RPE cells), and this is what occurs in human retinitis pigmentosa, glaucoma, and AMD, respectively. In recent studies utilizing animal and cell culture models, Cer accumulation has been established as one of the underlying causes of retinal cell death (26–28). Previously, using FTY720, a Cer synthase (CerS) inhibitor that blocks de novo light-induced Cer production (11, 29–31), we have shown that Cer plays a second-messenger role in the induction of retinal cell death, and that its inhibition can prevent and/or delay cell death (29). Therefore, targeting Cer could be a potential strategy for developing neuroprotective therapies for retinal diseases.

The enzyme group that hydrolyzes accumulated Cer into sphingosine (Sph) and releases free fatty acids is called ceramidase, also known as *N*-acylsphingosine amidohydrolase (ASAH). The lysosomal form of this enzyme is acid ceramidase, or ASAH1, and has very high expression in retinal and RPE cells [N. Mandal, unpublished observations; (6)]. The lysosomal breakdown of Cer into Sph is the major source for intracellular Sph 1-phosphate (S1P) production, which has an opposing role to Cer and provides cytoprotection (32, 33). We hypothesize that elevated ceramidase activity will reduce endogenous Cer levels, thereby protecting the cells from Cer-induced apoptosis.

In this study, we show that Cer and hexosyl-Cer (Hex-Cer) levels increase in ARPE19 cells that are oxidatively stressed by hydrogen peroxide (H₂O₂), and that overexpression of lysosomal ASAH1 can reduce the levels of both of these bioactive lipids. ARPE19 cells are immortalized human RPE cells that maintain their native epithelial properties and are extensively used in eye research. This study demonstrates, for the first time, that the overexpression of ASAH1 could help to protect human retinal cells from oxidative stress-induced cell death.

MATERIALS AND METHODS

Cell culture

ARPE19 cells, a human RPE cell line, were kindly supplied by Leonard Hjelmeland at University of California Davis. The cells

were maintained in a DMEM (Invitrogen-Gibco, Tokyo, Japan) containing 10% FBS (Invitrogen-Gibco), antibiotics (Invitrogen-Gibco), and L-glutamine (Invitrogen-Gibco), as described previously (34). The cultures were maintained at 37°C in a humidified atmosphere containing 95% air:5% CO₂.

Plasmid construction and introduction

cDNA of the known lysosomal transcript of human *ASAH1* (GenBank accession number BC016481.1) was cloned from ARPE19 cells. In order to construct expression vectors, cDNA encoding lysosomal *ASAH1* (Ly-*ASAH1*) was fused to the upstream DNA segment encoding the fluorescent protein, Venus (supplemental Fig. S1). Recombinant plasmids were linearized by restriction digestion and electroporated into ARPE19 cells (CUY21Pro-Vitro; NEPA GENE, Tokyo, Japan). Successful transgene expression of *ASAH1* was confirmed by assessing the expression of Venus fluorescence by microscopy (Axiovert 40; Carl Zeiss, Oberkochen, Germany), real-time PCR, and Western blotting. The localization of *ASAH1* in the cells was also investigated using a lysosomal marker, LysoTracker Red DND-99 (Invitrogen, Life Technologies Corp., Eugene, OR). Lysosomal *ASAH1* (Ly-*ASAH1*)-transduced cells were sorted with the excitation wavelength of 488 nm by Cell Sorter SH800 (Sony, Tokyo, Japan), and stably transfected ARPE19-*ASAH1* cells were selected.

Confocal laser scanning microscopy

For confocal laser scanning microscopy experiments, expression of *ASAH1* was confirmed by assessing the expression of Venus fluorescence using a Zeiss 710 confocal laser scanning microscope (Carl Zeiss). Localization of *ASAH1* in the cells was also investigated using a lysosomal marker, LysoTracker Red DND-99 (Invitrogen, Life Technologies Corp.). Live cells were seeded on glass coverslips and incubated with 500 nM of LysoTracker Red DND-99 for 2 h according to the manufacturer's instructions. Cells were then washed with 1 \times PBS, fixed with 4% paraformaldehyde for 15 min at room temperature, mounted in ProLong Diamond Antifade mountant with DAPI (Invitrogen, Life Technologies Corp.), and examined. Images were captured using ZEN 2012 imaging software (Carl Zeiss).

Western blots

Total cell lysates were used for Western blot analysis. Preparation of lysates was done utilizing T-PER tissue protein extraction reagent (Thermo Scientific, Rockford, IL) containing protease inhibitor (Roche, Indianapolis, IN) followed by brief sonication, centrifugation at 16,000 *g* for 10 min at 4°C, and supernatants stored at –20°C until needed. Protein estimation was performed utilizing a BCA assay (Thermo Scientific) for total protein concentration. Aliquots (~15 μ g) of protein samples were loaded on a 4–20% Tris-glycine gel (Novex; Life Technologies) for gel electrophoresis, transferred with a Bio-Rad Trans-Blot turbo transfer system to PVDF membrane (Bio-Rad, Hercules, CA), and membranes were incubated with Odyssey blocking buffer (TBS) (Licor, Lincoln, NE) for 1 h. Membranes were incubated with primary antibodies for anti-*ASAH1* (MilliporeSigma, Burlington, MA; 2 μ g/ml), anti-GFP (for the presence of Venus) (MilliporeSigma; 1:1,000), and β -actin (Abcam, Cambridge, MA; 1:5,000) overnight at 4°C and then incubated with appropriate secondary antibodies for 1 h at 4°C. Proteins were visualized by ECL detection (Pierce; Thermo Scientific) and data were normalized against β -actin.

Cell proliferation assay

In order to measure rate of growth, ARPE19 and ARPE19-*ASAH1* cells were plated in 12-well plates at a concentration of 2×10^5 cells/plate in replication, and grown at 37°C for up to 48 h.

Cell numbers were counted at 24 and 48 h using a cell counter (TC20; Bio-Rad, Japan).

Oxidative stress and short-chain Cer cell viability assays

ARPE19 cells (1×10^4) were plated in 96-well plates and grown at 37°C for 24 h. They were cultured in serum-free medium containing 100–1,000 μM H_2O_2 (Santoku Chemical Industries Co., Tokyo, Japan). After 24 h of incubation, cell viability was assessed by using a CellTiter 96 aqueous nonradioactive cell proliferation assay kit (Promega, Madison, WI). In this kit, viable and living cells are quantified by measuring the absorbance of the assay plates at 490 nm following the addition of 3-(4,5-dimethylthiazol-2-yl)-5-(3-carboxymethoxyphenyl)-2-(4-sulfophenyl)-2H-tetrazolium, inner salt (MTS), which is reduced by metabolically active cells to yield a soluble formazan product. From preliminary and previous studies, we estimated that at least 800 μM of H_2O_2 were needed to induce measurable cell death within 24 h in ARPE19 cells (35). We used an application of 800–1,000 μM of H_2O_2 for 24 h to induce oxidative stress in ARPE19-ASAHI cells, and ARPE19 cells served as controls. For biochemical and molecular analyses, we treated the cells with 1,000 μM of H_2O_2 for 3 and 24 h, and harvested and froze the cells. Deionized water in place of H_2O_2 served as the vehicle (Veh) for Veh-treated groups. Additionally, ARPE19 cells were grown per the methods stated above and were treated with exogenous C2-Cer dissolved in ethanol (Avanti Polar Lipids, Alabaster, AL) at concentrations of 10–50 μM , and an equivalent amount of ethanol-treated (100%) cells served as controls. Estimations based on preliminary data suggested that 20 μM of C2-Cer was sufficient to induce measurable cell death within 24 h in ARPE19 cells. ARPE19 and ARPE19-ASAHI cells were then treated with 10–20 μM of C2-Cer for 24 h and cell viability was determined per the methods stated above. To supplement the CellTiter viability assay, cell viability following H_2O_2 -induced oxidative stress, as described above, was determined indirectly in a repeated experiment by measuring released lactate dehydrogenase (LDH) into the medium using a commercial kit from Promega (CytoTox-One homogenous membrane integrity assay kit) following the manufacturer's instructions. For the LDH release assay, fluorescent measure of the release of LDH from cells with a damaged membrane was calculated by subtraction of culture medium background and the cell viability (percent) was calculated from 100% viability (mean value of untreated cells) to 0% viability (mean value of 2% Triton X-100-treated cells).

Quantitative analysis of sphingolipids

Sphingolipids were analyzed in the Lipidomics Core facility at Virginia Commonwealth University, Richmond, VA following previously established procedures (36). All internal standards were procured from Avanti Polar Lipids and added to samples at a ratio of ethanol:methanol:water (7:2:1) as a cocktail of 500 pmol each. Standards for sphingoid bases and sphingoid base 1-phosphates included the 17-carbon chain length analogs: C17-Sph, (2S,3R,4E)-2-aminoheptadec-4-ene-1,3-diol (d17:1-So); C17-sphinganine, (2S,3R)-2-aminoheptadecane-1,3-diol (d17:0-Sa); C17-S1P, heptadecaspHING-4-enine-1-phosphate (d17:1-So1P); and C17-sphinganine 1-phosphate, heptadecaspHINGanine-1-phosphate (d17:0-Sa1P). Standards for *N*-acyl sphingolipids were the C12-fatty acid analogs: C12-Cer, *N*-(dodecanoyl)-sphING-4-enine (d18:1/C12:0); C12-Cer 1-phosphate, *N*-(dodecanoyl)-sphING-4-enine-1-phosphate (d18:1/C12:0-Cer1P); C12-SM, *N*-(dodecanoyl)-sphING-4-enine-1-phosphocholine (d18:1/C12:0-SM); and C12-glucosylceramide, *N*-(dodecanoyl)-1- β -glucosyl-sphING-4-enine. MS grade solvents [chloroform (EM-CX1050), methanol (EM-MX0475), and formic acid (ASC grade, EM-FX0440-7)] were obtained from VWR (West Chester, PA).

Sphingolipid extraction was performed according to previously established procedures (11, 29, 36). Briefly, samples were added to 1 ml of CH_3OH and 0.5 ml of CHCl_3 , along with internal standards, into 13×100 mm borosilicate tubes with a Teflon-lined cap (60827-453; VWR). Samples were dispersed using an ultra sonicator for 30 s at room temperature. The single phase mixture was then incubated overnight at 48°C. After cooling, 75 μl of 1 M KOH in CH_3OH were added to the mixture, briefly sonicated, and then incubated in a shaking water bath at 37°C for 2 h to cleave potentially interfering glycerolipids. The extract was then brought to a neutral pH with 6 μl of glacial acetic acid, centrifuged, and the supernatant was collected and transferred into a new tube, where a SpeedVac was used to dry the extract. The dried extract was reconstituted in 0.5 ml of starting mobile phase solvent for LC/MS, sonicated for 15 s, and centrifuged. The supernatant was collected and transferred to the autoinjector vial for analysis.

Complex sphingolipids, sphingoid bases, and sphingoid base 1-phosphates were separated by reverse-phase LC with a Supelco 2.1 (internal diameter) \times 50 mm Ascentis Express C18 column (Sigma-Aldrich) and a binary solvent system at a flow rate of 0.5 ml/min with the column oven set at 35°C. The column was equilibrated with a solvent mixture of 95% mobile phase A1 ($\text{CH}_3\text{OH}/\text{water}/\text{HCOOH}$, 58:41:1, v/v/v, with 5 mM ammonium formate) and 5% mobile phase B1 ($\text{CH}_3\text{OH}/\text{HCOOH}$, 99:1, v/v, with 5 mM ammonium formate) for 0.5 min, and after a typical sample injection of 40 μl , the A1:B1 ratio was maintained at 95:5 for 2.25 min, followed by a linear gradient to 100% B1 over 1.5 min, which was held at 100% B1 for 5.5 min, followed by a 0.5 min gradient return to 95:5 A1:B1. Re-equilibration of the column with 95:5 A1/B1 for 0.5 min was done before the next run.

Confirmation and quantification of individual species of sphingolipids was performed using a Shimadzu LC-20 AD binary pump system coupled to a SIL-20AC autoinjector and a DGU20A3 degasser coupled to an ABI 4000 quadrupole/linear ion trap (QTrap) (Applied Biosystems) operating in triple quadrupole mode. Sphingolipid species, Cer, Hex-Cer, lactosyl-Cer (Lac-Cer), SM, and sphingoid lipids, such as Sph, dihydro-Sph (dh-Sph), S1P, and dihydro-S1P, were identified based on their retention time and *m/z* ratio and quantified, as described previously (37, 38), by comparing the target lipid ion of interest with the normalization of quantitated ion abundances. Quantitative lipid analyses for each sample were performed after normalizing against their levels of SM, which was selected due to its consistency as a structural sphingolipid.

RT-PCR

Total RNA extraction was carried out on harvested cells using the Ambion RNA mini extraction kit (Ambion TRIzol® Plus RNA purification kit; Life Technologies, Carlsbad, CA). The cDNA synthesis was followed by SuperScript™ III First-Strand Synthesis SuperMix (Invitrogen, Carlsbad, CA), according to the manufacturer's protocol. Primers for quantitative RT-PCR were designed in such a way that they spanned at least one intron, eliminating the chance of amplification from residual DNA contamination. The sequence of the primers is available from the corresponding author upon request. Expression of *ASAHI*, other sphingolipid metabolic genes, and oxidative and apoptotic marker genes were assayed by SYBR Green methods, and quantitation was calculated by the comparative Ct (threshold cycle) value method, as previously described (11, 39–43).

Data analysis and statistics

Data analysis and statistics for the sample sets were done by Student's *t*-test and two-way ANOVA, as appropriate, using GraphPad

RESULTS

Generation of stably transfected ARPE19-ASAHI cells

We generated an ARPE19 cell line stably transfected with the recombinant human *ASAHI* gene, henceforth referred to as ARPE19-ASAHI. Expression of the transgenic *ASAHI* was confirmed by immunocytochemical assays (Fig. 1A–D). The transgenic *ASAHI* protein colocalized with lysosomal marker in punctate structures, which is characteristic of lysosomal localization, confirming its cellular location (Fig. 1A–D). This localization pattern of *ASAHI* protein is consistent with previous findings (44). Stably transfected ARPE19-ASAHI cells were selected based

on Venus expression, propagated, and used in further experiments. The transgene expression of *ASAHI* was confirmed via fluorescence microscopy and RT-PCR and a significant increase of *ASAHI* mRNA was seen in ARPE19-ASAHI cells compared with ARPE19 cells (Fig. 1E; $P < 0.001$). Endogenous *ASAHI* protein expression was noted in both transfected and untransfected ARPE19 cells (Fig. 1F). *ASAHI* protein expression was more than doubled in ARPE19-ASAHI cells relative to ARPE19 cells (Fig. 1G; $P < 0.001$).

ASAHI activity tested by its effect on C2-Cer

In order to determine the activity and function of transgenic *ASAHI* in ARPE19 cells, we treated both ARPE19-ASAHI and ARPE19 control cells with exogenous short-chain C2-Cer. C2-Cer is known to cause cell death and our data showed a trend of decreasing cell viability with an increasing concentration of C2-Cer (Fig. 2A). A significant decrease

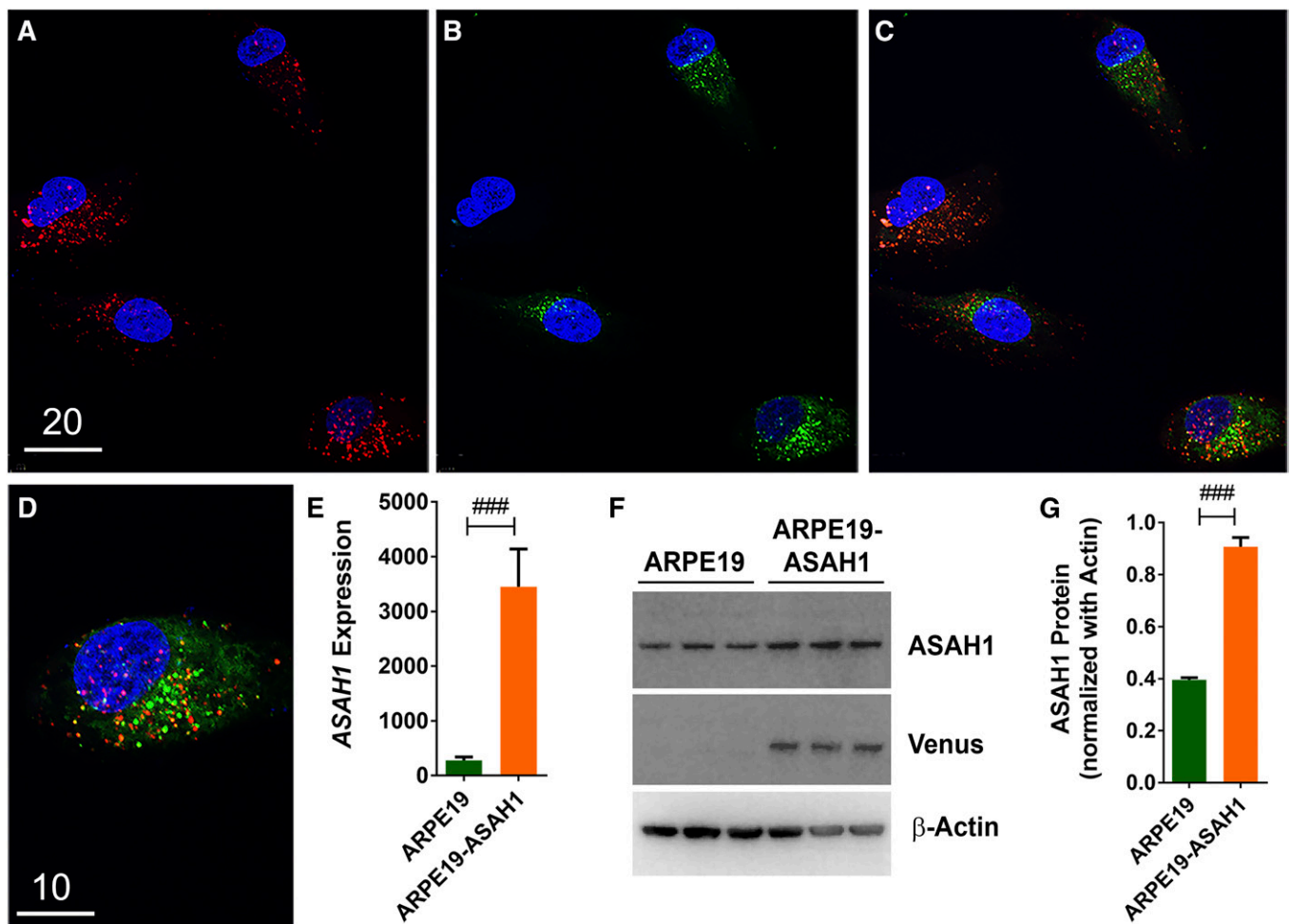


Fig. 1. Generation of *ASAHI*-expressed ARPE19 cells. Immunocytochemistry of *ASAHI*-expressed cells. *ASAHI* expression vector was electroporated into ARPE19 cells, and *ASAHI*-Venus-expressing cells were selected after sorting to develop stable pure culture. A: Cells were stained with a lysosomal marker, LysoTracker Red. B: Venus (green) expression was observed in *ASAHI* cells. C: Venus-*ASAHI* expression was majorly colocalized with the lysosomal marker. D: Enlarged image of *ASAHI* expression with LysoTracker Red; *ASAHI* shows cytoplasmic expression and ultimately moving to the punctate lysosomes. Scale bars: 20 μm (A–C) and 10 μm (D). E: Transgene expression was confirmed by RT-PCR, and a 10-fold increase in *ASAHI* was seen compared with ARPE19. F: Protein expression indicates endogenous *ASAHI* expression in both transfected and untransfected ARPE19 cells. G: *ASAHI* protein levels were normalized against β -actin, showing a >2-fold increase in *ASAHI* expression. ### $P < 0.001$ between cell lines.

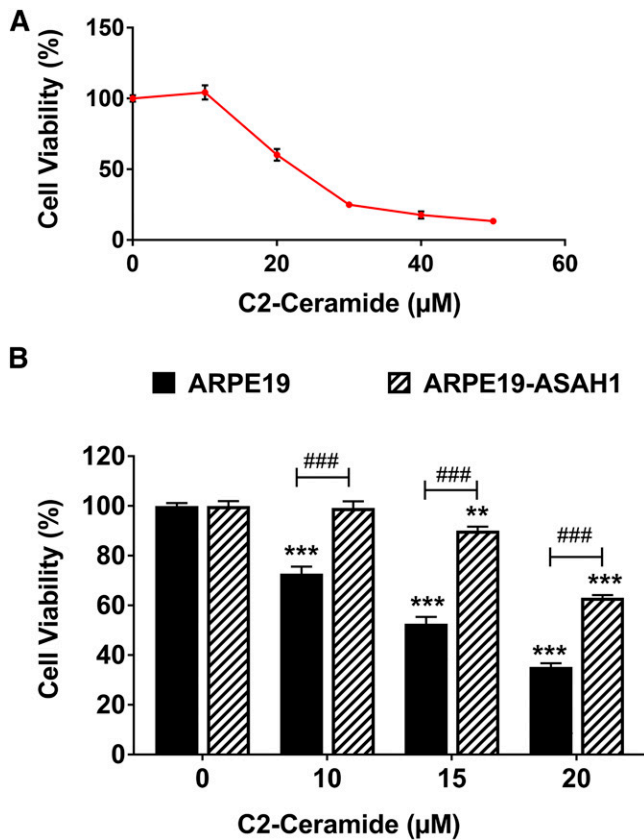


Fig. 2. Overexpression of Ly-ASAHI protects against short-chain Cer-mediated cell death. **A:** ARPE19 cells were treated with exogenous short-chain C2-Cer, which mimics the biological activity of endogenous Cer species. Treatment with C2-Cer concentrations over 20 μM for 24 h was sufficient to induce significant reductions in cell viability. **B:** ARPE19 cells and ARPE19 cells transfected with Ly-ASAHI were subjected to 10–20 μM C2-Cer concentrations for 24 h in serum-free media. Increasing C2-Cer concentration was correlated with decreasing cell viability for both ARPE19 cells and ARPE19-ASAHI cells, but ARPE19-ASAHI cells demonstrated resistance to Cer-mediated cell death at up to 10 μM C2-Cer. Cell viability was higher in ARPE19-ASAHI cells relative to ARPE19 cells at all concentrations of C2-Cer. ARPE19, $n = 4$; ARPE19-ASAHI, $n = 4$; *** $P < 0.01$ and *** $P < 0.001$ between treatment groups belonging to the same cell line; ### $P < 0.001$ between cell lines in a given treatment group.

in cell viability and an increase in cell death was noted beginning at a concentration of 10 μM C2-Cer ($P < 0.001$; Fig. 2A, B). ARPE19-ASAHI cells exhibited an apparent resistance to C2-Cer treatments at every dose. ARPE19-ASAHI viability was significantly higher than ARPE19 at all concentrations of C2-Cer ($P < 0.001$; Fig. 2B). This result suggests that overexpression of ASAHI can actively degrade C2-Cer and protect the cells from its lethal effect.

Characterization of ARPE19-ASAHI cells

ASAHI is the major Cer-hydrolyzing enzyme in cells; it hydrolyzes Cer to Sph, which serves as the major source of cellular SIP. Overexpression of ASAHI is expected to shift the cellular Cer/SIP balance toward increasing SIP, which is a well-established factor for cell growth and proliferation. Therefore, we analyzed whether the growth and proliferation

of the ARPE19-ASAHI cells are different from the native ARPE19 cells. We seeded an equal number of both ARPE19 and ARPE19-ASAHI cells, counted the cell numbers after 24 and 48 h of culture, and found that the numbers of ARPE19-ASAHI are 35–40% higher than ARPE19 cells (Fig. 3A). To evaluate the sphingolipid profiles in these cells, we harvested the cells after 48 h and assessed sphingolipid levels (picomoles per 10^6 cells; Fig. 3B, C). In the ARPE19-ASAHI cells, there was no significant increase in Cer 48 h after plating. However, a significant decrease was observed in Hex-Cer ($P < 0.001$) and SM ($P < 0.01$) at this time point (Fig. 3B), indicating that the synthesis of the Hex-Cer and SM was not favored in order to maintain the cellular pool of total Cer. Another reason for this difference may have been the catabolism of Hex-Cer and SM to maintain optimum cellular levels of Cer.

When we analyzed changes in the major intracellular lyso-sphingolipid species 48 h after plating, we found a significant increase in Sph (>2-fold; $P < 0.001$) and dh-Sph ($P < 0.001$) in ARPE19-ASAHI cells compared with ARPE19 cells (Fig. 3C). This increase likely resulted from the breakdown of Cer to Sph in the lysosome by the overexpressed ASAHI enzyme, and it suggests an active and functionally higher level of ASAHI in ARPE19-ASAHI cells. However, we did not see any changes in the SIP levels in these cells (Fig. 3C). In order to determine whether SIP was being secreted from the cells into the media, we harvested and analyzed the serum-free culture media of these cells and found moderate decreases in Cer, Hex-Cer, and SIP levels, as well as an increase in Sph levels (supplemental Fig. S2; $P < 0.05$). These data suggest that overexpression of ASAHI increases Sph levels and reduces both Hex-Cer and SM levels. However, we did not note changes in SIP levels, which we believe to be due to higher levels of SIP present in the serum-containing media in which the cells were cultured.

ASAHI overexpression protects ARPE19 cells from oxidative stress

In subsequent experiments, ARPE19-ASAHI and wild-type ARPE19 cells were exposed to H_2O_2 for 24 h to induce oxidative stress in serum-free media. After incubation, cell viability in ARPE19 cells was assessed using a cell proliferation assay. ARPE19 cells were resistant to low levels of oxidative stress, but viability decreased significantly starting at 800 μM H_2O_2 (Fig. 4A). Next, cell viability between ARPE19 and stably transfected ARPE19-ASAHI cells was compared (Fig. 4B). Cells were treated for 24 h with either 800, 900, or 1,000 μM of H_2O_2 . In the ARPE19 cells, there was a significant increase in cell death with increasing H_2O_2 concentration (800 μM , $P < 0.001$; 900 μM , $P < 0.001$; 1,000 μM , $P < 0.001$; Fig. 4B). Likewise, the ARPE19-ASAHI cells treated with H_2O_2 showed a dose-dependent increase in cell death (800 μM , $P < 0.001$; 900 μM , $P < 0.001$; 1,000 μM , $P < 0.001$). However, cell viability was significantly greater in ARPE19-ASAHI cells compared with the control ARPE19 cells at each dose of H_2O_2 (Fig. 4B; 800 μM , $P < 0.001$; 900 μM , $P < 0.001$; 1,000 μM , $P < 0.001$). Viability was reassessed using a LDH assay, which returned similar results. Specifically, ARPE19-ASAHI cytotoxicity was significantly

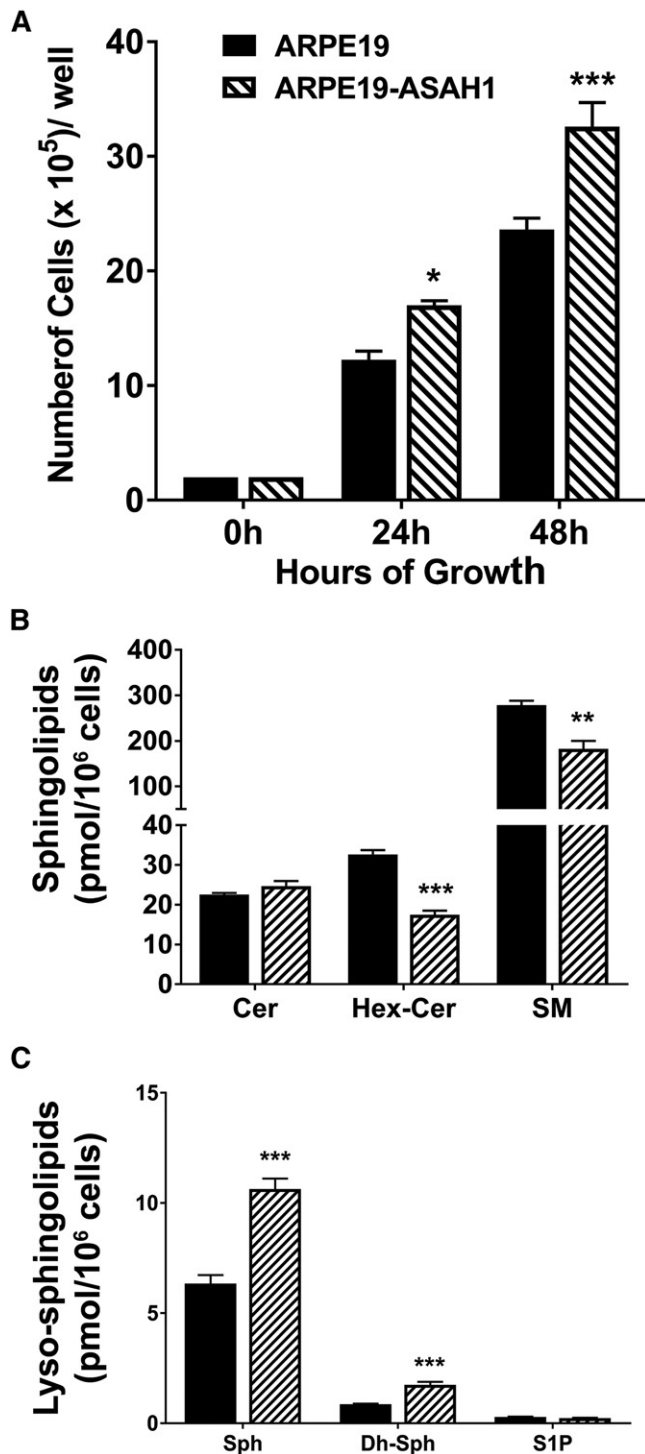


Fig. 3. Analysis of major sphingolipid content in untreated ARPE19 and ARPE19-ASAHI cells. A: ARPE19 and ARPE19-ASAHI cells were counted 24 and 48 h after culturing, with ARPE19-ASAHI cells being significantly more numerous than ARPE19 cells at 24 and 48 h. B: Bar graphs represent mean overall sphingolipid concentrations (pmol/million cells) \pm SEM. There was significantly less total Hex-Cer and SM in ARPE19-ASAHI cells after 48 h. C: Bar diagram comparing mean \pm SEM lyso-sphingolipid species (pmol/million cells). ARPE19-ASAHI cells had greater levels of Sph and dh-Sph compared with ARPE19 cells. ARPE19, n = 4; ARPE19-ASAHI, n = 4. * P < 0.05; P < 0.01; *** P < 0.001 between cell lines.

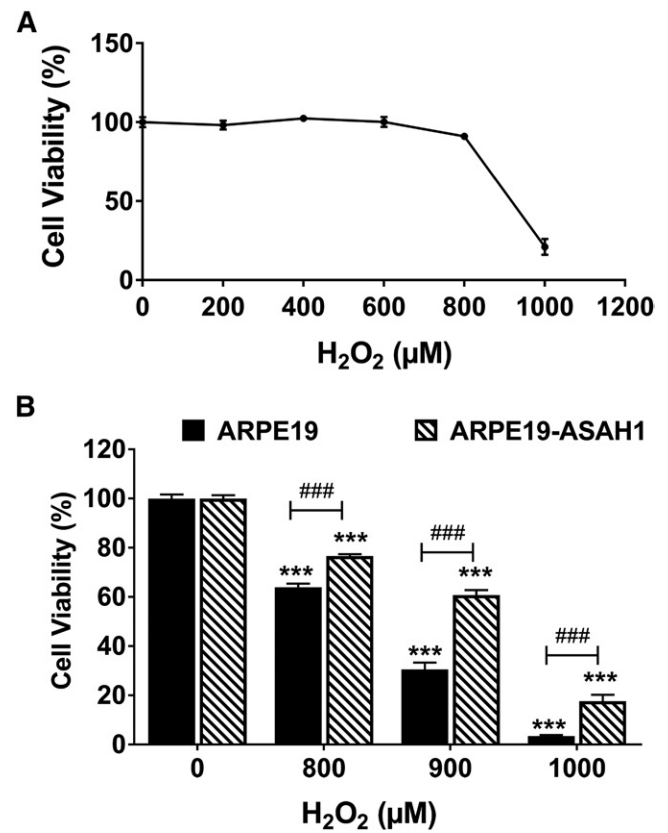


Fig. 4. Overexpression of Ly-ASAHI protects cells against oxidative cell death. A: ARPE19 cells underwent cell death following a concentration greater than 800 μ M H₂O₂. B: Bar diagrams depicting mean \pm SEM. Cells stably transfected with Ly-ASAHI (ARPE19-ASAHI) had significantly greater cell viability with an increase in oxidative stress. ARPE19, n = 4; ARPE19-ASAHI, n = 4. *** P < 0.001 between H₂O₂ concentrations; ### P < 0.001 between cell groups.

lower at all concentrations below 800 μ M of H₂O₂ (P < 0.05; supplemental Fig. S3). These results clearly indicate that ASAHI overexpression has a protective effect in ARPE19 cells from oxidative stress.

Analysis of cellular sphingolipids

We evaluated the absolute and relative composition of the major cellular sphingolipids (e.g., Cer, Hex-Cer, Lac-Cer, SM, and their subspecies), as well as cellular lyso-sphingolipids (e.g., Sph, dh-Sph, and S1P), in ARPE19 and ARPE19-ASAHI cells with and without H₂O₂ treatment. As mentioned earlier, cellular bioactive sphingolipids serve as signaling mediators. Hence, we analyzed the cells after 3 h of H₂O₂ treatment, when cell death was not yet evident.

Quantitative analysis of major sphingolipids. To understand how H₂O₂-induced oxidative stress affects sphingolipids in RPE cells, we measured total Cer, Hex-Cer, Lac-Cer, SM, and lyso-sphingolipid levels after 3 h of oxidative stress, before cell death became apparent. We normalized all sphingolipid data using SM, based on the fact that SM levels normalized to milligrams of protein remained unchanged between the two cell lines and with H₂O₂ treatment for 3 h (Fig. 5A). We found a significant increase in total Cer after H₂O₂ treatment in both ARPE19 (P < 0.001) and

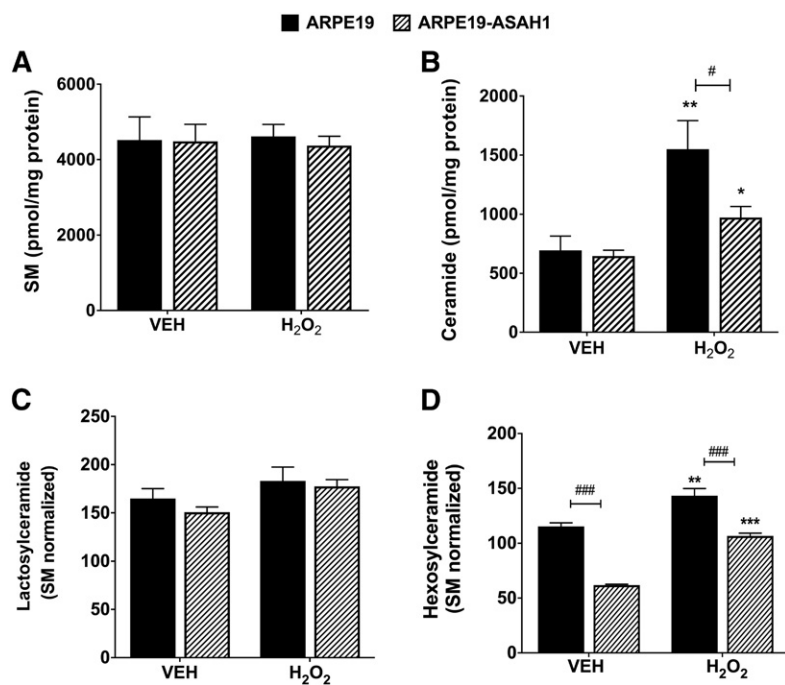


Fig. 5. Analysis of major sphingolipids with oxidative stress for 3 h. A: Bar diagram of mean total SM \pm SEM normalized with protein. No difference was observed between ARPE19 cells and ARPE19 cells transfected with Ly-ASAHI, nor was any difference observed between Veh-treated cells and cells under oxidative stress conditions for either group. B: Bar diagram of mean total Cer \pm SEM, normalized with protein. Veh-treated cells had no significant differences, but H₂O₂ treatment significantly increased Cer in both ARPE19 ($P < 0.01$) and ARPE19-ASAHI ($P < 0.05$) cells, but oxidatively stressed ARPE19-ASAHI cells had significantly lower Cer levels relative to ARPE19 cells ($P < 0.05$). C: Bar diagram of mean total Lac-Cer \pm SEM. No significant changes were seen in Lac-Cer levels between the ARPE19 cells and ARPE19-ASAHI cells or following oxidative stress in either group. D: Bar diagram of mean total Hex-Cer \pm SEM. ARPE19 cells with Veh treatment exhibited significantly higher levels of Hex-Cer relative to ARPE19-ASAHI cells. Following oxidative stress, the Hex-Cer levels increased significantly among both ARPE19 and ARPE19-ASAHI cells, while the ARPE19-ASAHI cells maintained significantly lower Hex-Cer levels relative to the H₂O₂-treated ARPE19 cells. ARPE19, $n = 4$; ARPE19-ASAHI, $n = 4$. * $P < 0.05$, ** $P < 0.01$, and *** $P < 0.001$ between H₂O₂ concentrations. # $P < 0.05$ and ### $P < 0.001$ between cell groups.

ARPE19-ASAHI cells ($P < 0.01$; Fig. 5B). However, overexpression of ASAHI significantly decreased the total Cer in ARPE19-ASAHI cells compared with ARPE19 cells in untreated cells ($P < 0.05$) and in oxidatively stressed cells ($P < 0.001$, Fig. 5B). Both protein and SM normalization resulted in similar patterns of changes in all other lipids, and because SM was an internal control for each sample, SM was used for normalizing all the lipids henceforth. We did not see any significant differences in Lac-Cer levels between the ARPE19 cells and the ARPE19-ASAHI cells with or without oxidative stress (Fig. 5C). However, we found that, in untreated cells, total Hex-Cer levels were significantly decreased in ARPE19-ASAHI versus ARPE19 cells ($P < 0.001$; Fig. 5D). Hex-Cer was increased after H₂O₂ treatment in both cell types, but was significantly less elevated in ARPE19-ASAHI cells ($P < 0.001$; Fig. 5D). In summary, overexpression of ASAHI appears to significantly reduce the levels of both Cer and Hex-Cer in untreated ARPE19 cells, while H₂O₂ treatment increased the levels of these sphingolipids, supporting our hypothesis that cellular Cers increase during oxidative stress and serve as second messengers to induce cell death, as reduction of these Cers reduces cell death.

Quantification of bioactive lyso-sphingolipid species in ARPE19 and ARPE19-ASAHI cells. Among the lyso-sphingolipids, we found Sph levels to be significantly higher in Veh-treated ARPE19-ASAHI compared with ARPE19 cells ($P < 0.001$; Fig. 6). There was no difference in the Sph levels between the two cell lines after oxidative stress, but H₂O₂ treatment significantly decreased Sph to roughly the same levels in both cell types ($P < 0.001$; Fig. 6). We detected higher levels of dh-Sph in ARPE19-ASAHI compared with ARPE19 in Veh-treated cells ($P < 0.01$; Fig. 6). Following

oxidative stress, there was no significant difference between the ARPE19 and ARPE19-ASAHI cell lines, but there was a significant increase in dh-Sph levels in the ARPE19 cells ($P < 0.05$; Fig. 6). We then measured the S1P levels and found that H₂O₂ treatment significantly increased S1P levels in both cell types ($P < 0.001$; Fig. 6); however, S1P levels were significantly reduced in ARPE19-ASAHI cells compared with ARPE19 cells for both treatments ($P < 0.001$ and $P < 0.01$, respectively; Fig. 6). The lyso-sphingolipid, Sph, can induce cell senescence and S1P signals for cell survival. Finding major changes in cellular S1P levels following oxidative stress suggests its association with cell death and survival.

Analysis of specific Cer and Hex-Cer species in ARPE19 and ARPE19-ASAHI cells. The different species of Cer and its metabolites play varied roles in cellular processes, including stress response. Therefore, we studied the effects of oxidative stress via H₂O₂ treatment on specific Cer species in ARPE19 and ARPE19-ASAHI cells. Following oxidative stress, there was an overall increase in long-chain Cer that occurred in both cell types. In ARPE19 cells, there were significant increases in C18:0 ($P < 0.001$), C20:0 ($P < 0.01$), C22:0 ($P < 0.05$), C24:1 ($P < 0.001$), C24:0 ($P < 0.01$), 26:1 ($P < 0.05$), and C26:0 levels ($P < 0.01$) following H₂O₂ treatment (Table 1). Likewise, in ARPE19-ASAHI cells there was a significant increase in C18:0 ($P < 0.001$), C22:0 ($P < 0.001$), C24:1 ($P < 0.01$), and C26:0 ($P < 0.01$; Table 1). However, ASAHI overexpression significantly decreased levels of Cer C16:0 ($P < 0.001$), C24:1 ($P < 0.01$), and C26:0 ($P < 0.05$) in the Veh treatment, and also decreased levels of C20:0 ($P < 0.05$), C24:1 ($P < 0.01$), C24:0 ($P < 0.05$), and C26:0 ($P < 0.05$) following H₂O₂ treatment (Table 1).

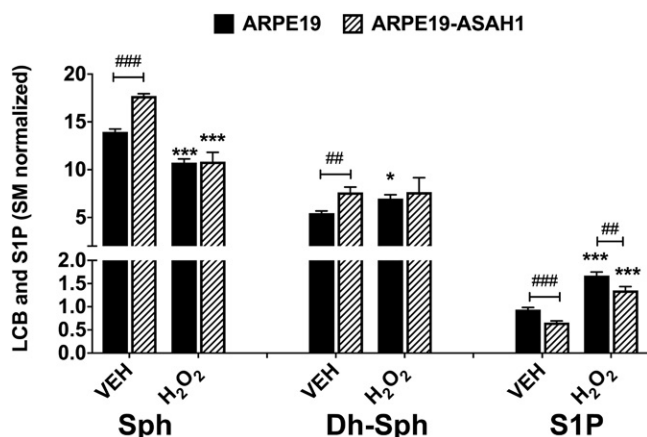


Fig. 6. Quantification of bioactive sphingoid species in ARPE19 and ARPE19-ASAHI cells. Bar diagrams depict mean \pm SEM of Sph, dh-Sph, and S1P content within ARPE19 and ARPE19-ASAHI cells. An oxidative stress-dependent effect was observed in both cell types. H₂O₂ treatment significantly reduced the content of Sph in both cell types. dh-Sph content within ARPE19 cells was significantly lower than dh-Sph levels in ARPE19-ASAHI cells, but increased following oxidative stress. S1P content was significantly lower in Veh-treated ARPE19-ASAHI cells. A significant increase in S1P was seen in an oxidative stress-dependent manner in both cell types, with ARPE19-ASAHI cells containing relatively lower levels of S1P among both treatment groups. Significant difference between Veh and H₂O₂ groups: * P < 0.05, *** P < 0.001; significant difference between ARPE19 and ARPE19-ASAHI cells: ## P < 0.01, ### P < 0.001; n = 4/group.

Interestingly, when we analyzed the Hex-Cer species, following the total Hex-Cer levels, we found significantly lower levels of major Hex-Cer species in Veh-treated ARPE19-ASAHI cells relative to ARPE19 cells: C14:0 (P < 0.05), C16:0 (P < 0.001), C18:1 (P < 0.01), C18:0 (P < 0.001), C20:0 (P < 0.01), C22:0 (P < 0.001), C24:1 (P < 0.001), C24:0 (P < 0.001), and C26:1 (P < 0.05) (Table 2). H₂O₂ treatment significantly increased C18:0 (P < 0.01), C22:0 (P < 0.01), and C24:1 (P < 0.001) levels in ARPE19

cells (Table 2). In the ARPE19-ASAHI cells, there was a significant increase in C16:0 (P < 0.01), C20:0 (P < 0.01), C22:0 (P < 0.001), C24:1 (P < 0.001), and C24:0 (P < 0.001) levels, but a significant decrease in C26:0 (P < 0.01) when compared with Veh-treated ARPE19-ASAHI cells (Table 2).

Compositional analysis of sphingolipid species. The relative composition or mole percent of the specific Cer and Hex-Cer species was also assessed from the above analyses, and differences were found between ARPE19 and ARPE19-ASAHI cells with and without H₂O₂ treatment. In Veh-treated cells, compared with ARPE19-ASAHI, ARPE19 exhibited greater relative levels of C16:0 (P < 0.001) and C24:1 (P < 0.01), whereas ARPE19-ASAHI had greater levels of C18:0 (P < 0.05) and C24:0 (P < 0.01) (supplemental Fig. S4A, C). Among the H₂O₂-treated cells, ARPE19-ASAHI cells had a greater relative amount of C18:0 (P < 0.01) and C22:0 (P < 0.01) than the Veh-treated cells (supplemental Fig. S4B, D). Following oxidative stress, ARPE19 cells were found to have significantly reduced relative levels of C14:0 (P < 0.05), C16:0 (P < 0.01), and C26:0 (P < 0.001), but increased in relative C24:1 (P < 0.05) and C24:0 (P < 0.01) content (supplemental Fig. S4A, B). In ARPE19-ASAHI cells, H₂O₂ treatment increased both C18:0 (P < 0.001) and C24:1 (P < 0.01) and decreased C14:0 (P < 0.05), C24:0 (P < 0.05), and C26:0 (P < 0.01) (supplemental Fig. S4C, D).

When the relative composition of Hex-Cer was compared between Veh-treated cells, ARPE19 and ARPE19-ASAHI cells exhibited similar levels of all major Hex-Cer species aside from a depressed level of C24:0 (P < 0.05) in the Ly-ASAHI-transfected cells (supplemental Fig. S5A, C). Interestingly, after oxidative stress, ARPE19 was found to have a significantly reduced level of C24:0 (P < 0.01) relative to ARPE19-ASAHI cells (supplemental Fig. S5B, D). When the cells were treated with H₂O₂, ARPE19 cells had greater levels of C22:0 (P < 0.001), C24:1 (P < 0.001), and

TABLE 1. Composition of Cer from ARPE19 and ARPE19-ASAHI cells

Cer Species	ARPE19		ARPE19-ASAHI	
	Veh (3 h)	H ₂ O ₂ (3 h)	Veh (3 h)	H ₂ O ₂ (3 h)
C14:0	2.60 \pm 0.31	2.30 \pm 0.12	2.31 \pm 0.19	1.77 \pm 0.11
C16:0	13.75 \pm 0.66	11.88 \pm 0.66	8.19 \pm 0.35 ^d	9.95 \pm 0.53
C18:1	0.52 \pm 0.03	0.59 \pm 0.05	0.48 \pm 0.02	0.55 \pm 0.04
C18:0	1.46 \pm 0.11	3.06 \pm 0.11 ^b	1.75 \pm 0.10	3.50 \pm 0.15 ^b
C20:0	0.87 \pm 0.06	1.43 \pm 0.10 ^c	0.87 \pm 0.09	0.95 \pm 0.08 ^d
C22:0	8.68 \pm 0.87	12.01 \pm 0.85 ^e	7.89 \pm 0.21	11.30 \pm 0.36 ^b
C24:1	23.81 \pm 0.56	37.06 \pm 1.58 ^b	16.84 \pm 0.98 ^f	28.11 \pm 1.73 ^{c,f}
C24:0	32.77 \pm 1.05	54.21 \pm 3.58 ^e	35.19 \pm 1.30	40.36 \pm 1.51 ^d
C26:1	7.30 \pm 0.55	9.65 \pm 0.41 ^e	7.73 \pm 0.44	6.38 \pm 1.31
C26:0	2.94 \pm 0.18	1.52 \pm 0.27 ^e	2.04 \pm 0.19 ^d	0.72 \pm 0.10 ^{c,d}
Total	94.70 \pm 1.44	133.71 \pm 5.80 ^c	83.28 \pm 1.85 ^f	103.60 \pm 4.54 ^{c,f}

Cells were treated with Veh or H₂O₂ for 3 h. Absolute quantification (pmol \times 1,000) values (mean \pm SEM) presented for each species after being normalized with SM.

^a P < 0.001 between ARPE19 and ARPE19-ASAHI cells of same treatment group; n = 4/condition.

^b P < 0.001 between Veh and H₂O₂ treatment; n = 4/condition.

^c P < 0.01 between Veh and H₂O₂ treatment; n = 4/condition.

^d P < 0.05 between ARPE19 and ARPE19-ASAHI cells of same treatment group; n = 4/condition.

^e P < 0.05 between Veh and H₂O₂ treatment; n = 4/condition.

^f P < 0.01 between ARPE19 and ARPE19-ASAHI cells of same treatment group; n = 4/condition.

TABLE 2. Composition of Hex-Cer from ARPE19 and ARPE19-ASAHI cells

Hex-Cer Species	ARPE19		ARPE19-ASAHI	
	Veh	H ₂ O ₂ (3 h)	Veh	H ₂ O ₂ (3 h)
C14:0	3.75 ± 0.48	3.44 ± 0.45	2.44 ± 0.24 ^a	2.62 ± 0.11
C16:0	30.76 ± 0.77	32.56 ± 1.61	16.50 ± 1.21 ^b	22.57 ± 0.92 ^{c,d}
C18:1	0.58 ± 0.06	0.72 ± 0.11	0.31 ± 0.03 ^d	0.57 ± 0.07
C18:0	3.15 ± 0.09	4.02 ± 0.15 ^c	1.75 ± 0.09 ^b	3.52 ± 0.61
C20:0	0.96 ± 0.09	1.04 ± 0.05	0.47 ± 0.05 ^d	0.77 ± 0.05 ^{c,d}
C22:0	12.57 ± 0.29	23.31 ± 1.85 ^c	7.67 ± 0.48 ^b	15.93 ± 1.10 ^{a,e}
C24:1	11.25 ± 0.41	23.85 ± 1.01 ^c	5.44 ± 0.34 ^b	17.09 ± 1.22 ^{d,e}
C24:0	43.73 ± 1.25	48.75 ± 2.99	21.66 ± 0.42 ^b	40.07 ± 0.51 ^{a,e}
C26:1	2.91 ± 0.14	3.32 ± 0.39	1.82 ± 0.26 ^a	2.62 ± 0.11
C26:0	5.79 ± 1.45	2.21 ± 0.29	3.85 ± 0.69	1.06 ± 0.24 ^{a,c}
Total	115.44 ± 3.23	143.22 ± 6.65 ^c	61.89 ± 0.68 ^b	106.81 ± 2.45 ^{d,e}

Cells were treated with Veh or H₂O₂ for 3 h. Absolute quantification (pmol × 1,000) values (mean ± SEM) presented for each species after being normalized with SM.

^a*P* < 0.05 between ARPE19 and ARPE19-ASAHI cells of same treatment group; n = 4/condition.

^b*P* < 0.001 between ARPE19 and ARPE19-ASAHI cells of same treatment group; n = 4/condition.

^c*P* < 0.01 between Veh and H₂O₂ treatment; n = 4/condition.

^d*P* < 0.01 between ARPE19 and ARPE19-ASAHI cells of same treatment group; n = 4/condition.

^e*P* < 0.001 between Veh and H₂O₂ treatment; n = 4/condition.

C26:0 (*P* < 0.05), but lower levels of C16:0 (*P* < 0.001) and C24:0 (*P* < 0.01) (supplemental Fig. S5A, B). In H₂O₂-treated ARPE19-ASAHI cells, we observed increased levels of C22:0 (*P* < 0.05) and C24:1 (*P* < 0.01), as well as decreased levels of C14:0 (*P* < 0.05), C16:0 (*P* < 0.05), and C26:0 (*P* < 0.01) (supplemental Fig. S5C, D).

In summary, *ASAHI* overexpression resulted in significant changes in the relative composition of Cer and Hex-Cer species in ARPE19 cells, both of which have been found to be altered due to exposure to oxidative stress. However, this effect was less pronounced among the Hex-Cer species.

Expression of sphingolipid, apoptotic, and inflammatory genes

We utilized RT-PCR to analyze sphingolipid, inflammatory, and apoptotic genes in ARPE19 and ARPE19-ASAHI cells. As shown in Fig. 1E, expression of *ASAHI* in the stably transfected cells was significantly higher than in the wild-type ARPE19 cells (*P* < 0.001). A 2-fold increase in expression of *ASAHI* protein in ARPE19 cells transfected with *ASAHI* was confirmed through normalization with β-actin (*P* < 0.001; Fig. 1G). Treatment with H₂O₂ did not make a significant difference in the expression of *ASAHI* in these cells (supplemental Fig. S6). We further tested the expression of other sphingolipid metabolic genes. After 3 h of H₂O₂ treatment, there was a significant increase in serine palmitoyl transferase 2 (*SPT2*; *P* < 0.05) in ARPE19-ASAHI cells compared with ARPE19 cells (Fig. 7); yet, when comparing to ARPE19-ASAHI controls, oxidative stress resulted in a significant decrease in *SPT2* (*P* < 0.05; Fig. 7).

We tested the expression of a group of apoptotic and inflammatory genes in the above conditions. The genes we tested included proto-oncogene *C-Fos* (*cFOS*), FOS-like 1, B-cell CLL/lymphoma 2 (*BCL2*), *BCL2*-associated X protein, poly (ADP-ribose) polymerase (*PARP*), C-C motif chemokine ligand 2 (*CCL2*), intercellular adhesion molecule 1 (*ICAMI*), heme oxygenase (decycling) 1 (*HO-1*), *TNFα*, and interleukin 6 (Fig. 8). We detected differential expression

of *cFOS*, *PARP*, *ICAMI*, and *HO-1* in H₂O₂-treated ARPE19-ASAHI cells (Fig. 8). Expression of apoptotic *cFOS* and *BCL2* were significantly lower in H₂O₂-treated ARPE19-ASAHI cells, and expression of the inflammatory gene, *CCL2*, was significantly higher (Fig. 8) indicating that overexpression of *ASAHI* might have reduced the cell death process by reducing oxidative stress to these cells.

DISCUSSION

In the present study, we investigated how overexpression of lysosomal ceramidase (Ly-*ASAHI*) affects retinal cell death in vitro via oxidative stress. Oxidative stress is implicated in the etiology and pathogenesis of many neurodegenerative disorders, including the RD that occurs in retinitis pigmentosa, diabetic retinopathy, and AMD (45–49). In

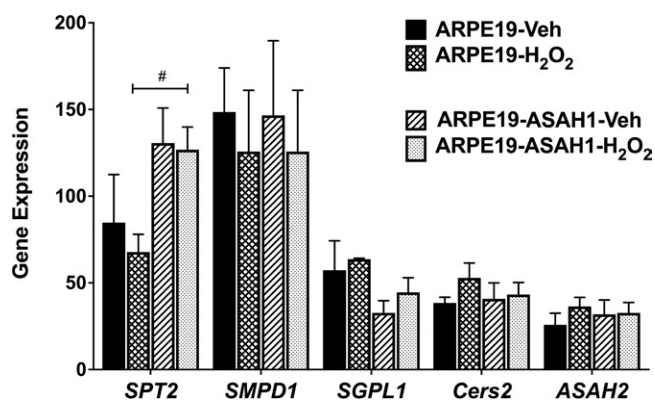


Fig. 7. RT-PCR analysis of sphingolipid metabolic genes with oxidative stress. Each sample included in a condition that consisted of three independent RT-PCR experiments that were averaged and normalized against housekeeping genes. Bar graphs are represented as mean ± SEM. Change in sphingolipid genes as a result of overexpressed *ASAHI* and stress condition. Significant difference between cell types depicted: #*P* < 0.05; n = 4. *SMPD1*, SM phosphodiesterase 1; *SGPL1*, S1P lyase 1; *Cers2*, Cer synthase 2.

■ ARPE19 ▨ ARPE19-H₂O₂ □ ARPE19-ASAHI ▩ ARPE19-ASAHI-H₂O₂

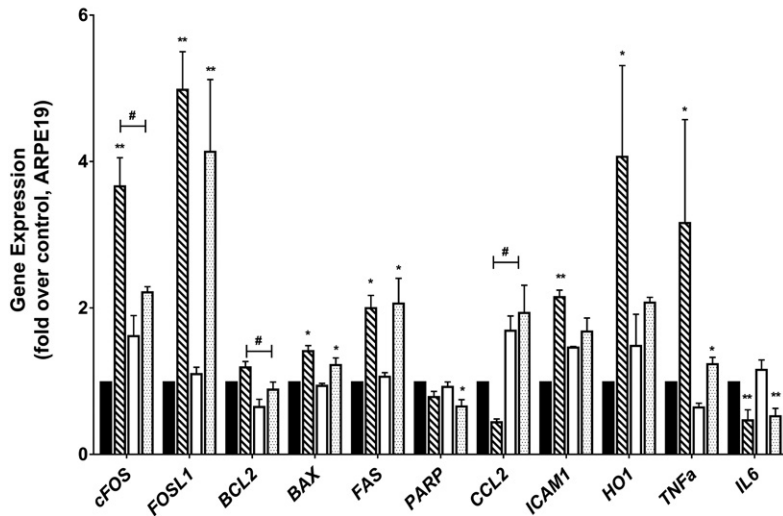


Fig. 8. RT-PCR analysis of inflammatory and apoptotic genes with oxidative stress. Each sample included in a condition that consisted of three independent RT-PCR experiments that were averaged and normalized against housekeeping genes. Bar graphs are represented as fold over control mean \pm SEM from $n = 6$ biological replications. Change in inflammatory and apoptotic markers as a result of cell type and oxidative stress. Significant difference between treatment groups: * $P < 0.05$, ** $P < 0.01$. Significant difference between cell types depicted: # $P < 0.05$. *FOSL1*, FOS-like 1; *BAX*, BCL2-associated X protein; *FAS*, Fas cell surface death receptor; *IL6*, interleukin 6.

AMD, for example, UV sunlight exposure and smoking generate reactive oxygen species in the RPE cells, which causes oxidative stress and is considered to be the major pathological cause of the disease (45, 46). However, the mechanism by which reactive oxygen species induce RPE cell death is not fully understood. It is well-documented that oxidative stress (e.g., light, chemical, and physical) can induce excess Cer biosynthesis, and we, along with other laboratories, recently established that Cer accumulation causes retinal cell death (11, 12, 29, 50). In this study, we found that ARPE19 cells overexpressing lysosomal ceramidase (ARPE19-ASAHI) were protected from H₂O₂-induced oxidative stress by reducing the levels of bioactive Cer and Hex-Cer and SIP levels. The SIP increase due to oxidative stress (Fig. 6) could very well be a consequence of higher levels of Cer that counteract the Cer action toward cell death. Cer inhibits cell growth and promotes apoptosis and senescence, whereas SIP induces cell proliferation and migration by signaling through one of five SIP receptors (51–53). This delicate balance, or rheostat, between these two molecules ultimately determines whether the cell undergoes apoptosis or proliferation (54). Consequently, targeting pathways that decrease Cer accumulation could be a promising therapeutic approach for treating or preventing RD, as we demonstrated in earlier studies (12, 29). This is the first report that uses a genetic means to reduce excess cellular Cer by stably overexpressing the ceramidase enzyme in mammalian cells, ultimately preventing oxidative stress-induced cell death.

In this study, we cloned the human *ASAHI* gene from ARPE19 cells, fused it with a fluorescent marker (Venus), and transfected it into the same cells, thereby generating stable ARPE19 cells that overexpressed the *ASAHI* gene (ARPE19-ASAHI; Fig. 1). We verified the expression of the transgene, the proper localization of the protein (lysosomes), and the function of the transgenic protein by lipid product analysis and its ability to protect cells from exogenous Cer-induced cell death (Figs. 1, 2). *ASAHI* overexpression resulted in significantly higher levels of Sph in

ARPE19 cells, and it reduced the levels of higher-order Cer anabolic products, such as Hex-Cers and SM (Fig. 3B, C). When we introduced oxidative stress to these cells, we observed significant protection of ARPE19-ASAHI cells from H₂O₂ compared with the ARPE19 cells (Fig. 4B). In ARPE19 cells, we further demonstrated that oxidative stress via H₂O₂ induces an increase in Cer and Hex-Cer species, which is significantly reduced by overexpression of *ASAHI*, thereby protecting the cells (Fig. 5).

We observed variability in the levels of individual Cer and Hex-Cer species in both cell types during oxidative stress (Tables 1, 2). Oxidative stress has been shown to induce de novo Cer biosynthesis (11, 27, 33, 55). Cellular Cers are synthesized by Cer synthases, and there are six different CerSs (CerS1–6) found in the mammalian system. The chain length of Cer depends on the activity of the specific CerS. CerS1 synthesizes mainly C18-Cer; CerS4 synthesizes C18-/C20-/C24-Cer; CerS5 and CerS6 synthesize mostly C14-/C16-/C18-Cer; CerS2 synthesizes preferentially C22-/C24-Cer; and CerS3 synthesizes very long-chain Cers (>C26-Cer) (36, 56–59). Our data may suggest an activation of CerS2 and an inhibition of CerS3. In summary, this study establishes that: 1) H₂O₂-mediated oxidative stress increases Cer in ARPE19 cells, which is one of the contributing factors of cell death; and 2) overexpression of *ASAHI* can prevent cell death by hydrolyzing excess Cer.

The mammalian *ASAHI* is a lysosomal enzyme, which is active in the acidic environment of the lysosome. The acidic subcellular compartments, the late endosomes, and the lysosomes are the sites for constitutive degradation of sphingolipids and glycosphingolipids, with the end goal being Sph production. We detected Venus-fused *ASAHI* expression in cytoplasm and late endosomes (not colocalized with LysoTracker) and in lysosomes (Fig. 1B–D). In the case of glycosphingolipids, the stepwise release of mono-saccharide units by exohydrolases occurs at an acidic pH, leaving just the Sph portion of the molecule (i.e., Cer). Cer can be further hydrolyzed by acid ceramidase (*ASAHI*) to form Sph and a free fatty acid, both of which are able to

leave the lysosome, unlike Cer. The salvage pathway reutilizes long-chain sphingoid bases to form Cer through the action of CerS at the surface of the ER or in ER-associated membranes. The salvage pathway has been estimated to contribute between 50% and 90% of sphingolipid biosynthesis, suggesting major associations between lysosomal degradation and recycling of sphingolipids in cells (60). ASAHI, being the ultimate enzyme in the lysosomal degradation pathway, plays an important role in mammalian cells. A mutation in the *ASAHI* gene causes Farber disease in humans (Farber's lipogranulomatosis), which is an in-born lipid storage disease characterized by Cer accumulation in tissue that results in early death (61). ASAHI plays an important role in balancing the levels of cellular Cer and S1P, and it was expected that an increase of ASAHI activity would facilitate cell survival, while a decrease in ASAHI activity would result in cell apoptosis. ASAHI deficiency in the mouse retina causes early cell death (N. Mandal, unpublished observations), whereas overexpression of ASAHI is associated with various human cancers, suggesting a role in cell proliferation (62). For the first time, we report in this study that overexpressing *ASAHI* decreases levels of Hex-Cer and increases levels of Sph, which possibly maintains the steady-state levels of Cer that are needed to maintain healthy cell growth.

This study also underscores the involvement of the Cer lipids downstream of H₂O₂ signaling. H₂O₂ inhibits cell growth and proliferation via the PI3K/AKT/mTOR and Erk signaling pathways. AKT/protein kinase B, a serine/threonine kinase, is a versatile pro-proliferative signaling protein activated by phosphorylation at Ser⁴⁷³ by phosphoinositide-dependent kinase 1 (PDK1). Akt activation, in turn, signals to a variety of key downstream targets, including GSK3β and mTOR, which consequently inhibits apoptosis and promotes cell survival in a regulated manner (63). Cer, a multifunctional central molecule in the sphingolipid biosynthetic pathway, exerts potent apoptotic effects in a variety of cell types (64–70), and it is one of the potent mediators of RD. Cer biosynthesis mainly occurs via: 1) the de novo pathway, 2) SMase-mediated hydrolysis of SM, and/or 3) the inhibition of ceramidase or glucosylceramide

synthase-mediated conversion of Cer into Sph and glucosylceramide into Cer, respectively. Cer-activated protein phosphatases, such as protein phosphatase 1 and protein phosphatase 2A, were shown to dephosphorylate Akt at Ser⁴⁷³, which ultimately led to the inactivation of AKT and the induction of apoptosis (71–76).

Significant differences in gene expression between the ARPE19 and ARPE19-ASAHI cells under oxidative stress serve to further demonstrate the importance of Cer metabolism in cell survival. In ARPE19-ASAHI cells under oxidative stress, *PARP* expression is significantly reduced (Fig. 8). This is notable, as *PARP* is involved in DNA excision repair, and elevations in *PARP* activation have been reported in apoptosis resulting from cerebral ischemia, inflammation, and oxidative stress injuries. *PARP* is also implicated in Cer-induced apoptosis (77). *cFOS*, a member of the AP-1 transcription factor complex associated with apoptotic cell death (78), was also significantly reduced in ASAHI-overexpressing cells. *Bcl2* family proteins involved with pro- and anti-apoptotic pathways (79) are also decreased in ARPE19-ASAHI cells compared with controls (Fig. 8). Inflammatory gene expression is also substantially influenced by oxidative stress and the activity of ASAHI, as evidenced by significant differences between ARPE19 and ARPE19-ASAHI expression of *CCL2*, *ICAM*, *HO-1*, and *TNFα* (Fig. 8), which are all involved in inflammation and/or apoptotic pathways (80–83). Clearly, ASAHI overexpression and the resultant disruption of sphingolipid metabolic processes has wide-ranging effects that include increased cell survival in oxidative stress through modulation of apoptotic and inflammatory pathways, though the mechanisms of these actions and Cer's exact role in them are yet to be fully established. Maintaining steady-state levels of Cer is essential for cell survival and growth, and the salvage pathway plays an important role in this balance. We found higher levels of Sph in ASAHI-ARPE19 cells, which suggests activation of the salvage pathway to maintain the cellular Cer level, as seen in our results (Figs. 3, 6). The salvage pathway, which generates Cer from Sph, is pro-survival, whereas ER stress is increased by an overly activated de novo pathway (84), which might have played a

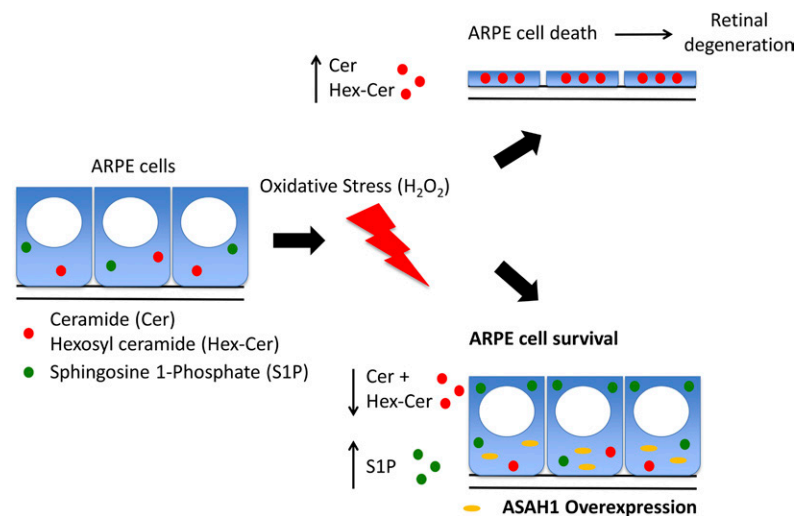



Fig. 9. Schematic model of bioactive sphingolipid regulation of ARPE cell viability under oxidative stress. Oxidative stress induced by H₂O₂ causes an increase in the levels of Cer and Hex-Cer species in ARPE cells and leads to cell death and subsequent RD. ARPE cell survival under oxidative stress can be achieved through overexpression of ASAHI.

major role in protecting ARPE19-ASAH1 cells from oxidative stress.

In conclusion, in our *in vitro* study using human immortal RPE cell lines, we have established that bio-active Cer plays a role in oxidative stress-induced cell death, which could ultimately be targeted to develop novel therapeutic treatments for human AMD and other degenerative diseases. These experiments suggest that overexpression of the *ASAH1* gene can help to protect RPE cells from cell death by metabolizing excess Cer (Fig. 9), which helps to justify further investigation into using or targeting Cer-modifying enzymes to protect retinal cells. The transgenic *ASAH1* overexpression strategy has been shown to be effective to prevent retinal photoreceptor degeneration in *Drosophila* (85), and we expect that this strategy could result in similar findings in higher organisms. Our future studies focusing on *ASAH1* gene therapy in the mammalian system will generate further valuable information on how this intracellular target (Cer) is associated with human retinal diseases, and how we can ultimately develop novel therapeutic strategies. 

The authors thank Dr. Rajashekhar Gangaraju from the Department of Ophthalmology, University of Tennessee Health Science Center, Memphis, TN 38163 for his generous gift of some quantitative RT-PCR primers.

REFERENCES

- Young, R. W. 1987. Pathophysiology of age-related macular degeneration. *Surv. Ophthalmol.* **31**: 291–306.
- Hogan, M. J. 1972. Role of the retinal pigment epithelium in macular disease. *Trans. Am. Acad. Ophthalmol. Otolaryngol.* **76**: 64–80.
- Holz, F. G., C. Bellman, S. Staudt, F. Schutt, and H. E. Volcker. 2001. Fundus autofluorescence and development of geographic atrophy in age-related macular degeneration. *Invest. Ophthalmol. Vis. Sci.* **42**: 1051–1056.
- Kennedy, C. J., P. E. Rakoczy, and I. J. Constable. 1995. Lipofuscin of the retinal pigment epithelium: a review. *Eye (Lond.)* **9**: 763–771.
- Tomita, H., T. Abe, and M. Tamai. 2000. Ceramide-induced cell death in cultured rat retinal pigment epithelial cells. *Tohoku J. Exp. Med.* **190**: 223–229.
- Kannan, R., M. Jin, M. A. Gamulescu, and D. R. Hinton. 2004. Ceramide-induced apoptosis: role of catalase and hepatocyte growth factor. *Free Radic. Biol. Med.* **37**: 166–175.
- Barak, A., L. S. Morse, and T. Goldkorn. 2001. Ceramide: a potential mediator of apoptosis in human retinal pigment epithelial cells. *Invest. Ophthalmol. Vis. Sci.* **42**: 247–254.
- Merrill, A. H., Jr., E. M. Schmelz, D. L. Dillehay, S. Spiegel, J. A. Shayman, J. J. Schroeder, R. T. Riley, K. A. Voss, and E. Wang. 1997. Sphingolipids—the enigmatic lipid class: biochemistry, physiology, and pathophysiology. *Toxicol. Appl. Pharmacol.* **142**: 208–225.
- Spiegel, S., and A. H. Merrill, Jr. 1996. Sphingolipid metabolism and cell growth regulation. *FASEB J.* **10**: 1388–1397.
- Jarvis, W. D., and S. Grant. 1998. The role of ceramide in the cellular response to cytotoxic agents. *Curr. Opin. Oncol.* **10**: 552–559.
- Chen, H., J. T. Tran, A. Eckerdt, T. P. Huynh, M. H. Elliott, R. S. Brush, and N. A. Mandal. 2013. Inhibition of *de novo* ceramide biosynthesis by FTY720 protects rat retina from light-induced degeneration. *J. Lipid Res.* **54**: 1616–1629.
- Chen, H., J. T. Tran, R. S. Brush, A. Saadi, A. K. Rahman, M. Yu, D. Yasumura, M. T. Matthes, K. Ahern, H. Yang, et al. 2012. Ceramide signaling in retinal degeneration. *Adv. Exp. Med. Biol.* **723**: 553–558.
- Jiang, P., M. Bian, W. Ma, C. Liu, P. Yang, B. Zhu, Y. Xu, M. Zheng, J. Qiao, Z. Shuai, et al. 2016. Eryptosis as an underlying mechanism in systemic lupus erythematosus-related anemia. *Cell. Physiol. Biochem.* **40**: 1391–1400.
- Checa, A., H. Idborg, A. Zandian, D. G. Sar, I. Surowiec, J. Trygg, E. Svenungsson, P. J. Jakobsson, P. Nilsson, I. Gunnarsson, et al. 2017. Dysregulations in circulating sphingolipids associate with disease activity indices in female patients with systemic lupus erythematosus: a cross-sectional study. *Lupus.* **26**: 1023–1033.
- Galadari, S., A. Rahman, S. Pallichankandy, A. Galadari, and F. Thayyullathil. 2013. Role of ceramide in diabetes mellitus: evidence and mechanisms. *Lipids Health Dis.* **12**: 98.
- Xing, Y., Y. Tang, L. Zhao, Q. Wang, W. Qin, X. Ji, J. Zhang, and J. Jia. 2016. Associations between plasma ceramides and cognitive and neuropsychiatric manifestations in Parkinson's disease dementia. *J. Neurol. Sci.* **370**: 82–87.
- Abbott, S. K., H. Li, S. S. Munoz, B. Knoch, M. Batterham, K. E. Murphy, G. M. Halliday, and B. Garner. 2014. Altered ceramide acyl chain length and ceramide synthase gene expression in Parkinson's disease. *Mov. Disord.* **29**: 518–526.
- Biennias, K., A. Fiedorowicz, A. Sadowska, S. Prokopiuk, and H. Car. 2016. Regulation of sphingomyelin metabolism. *Pharmacol. Rep.* **68**: 570–581.
- Young, S. A., J. G. Mina, P. W. Denny, and T. K. Smith. 2012. Sphingolipid and ceramide homeostasis: potential therapeutic targets. *Biochem. Res. Int.* **2012**: 248135.
- Katsel, P., C. Li, and V. Haroutunian. 2007. Gene expression alterations in the sphingolipid metabolism pathways during progression of dementia and Alzheimer's disease: a shift toward ceramide accumulation at the earliest recognizable stages of Alzheimer's disease? *Neurochem. Res.* **32**: 845–856.
- de la Monte, S. M., E. Re, L. Longato, and M. Tong. 2012. Dysfunctional pro-ceramide, ER stress, and insulin/IGF signaling networks with progression of Alzheimer's disease. *J. Alzheimers Dis.* **30** (Suppl. 2): S217–S229.
- Chatterjee, M., and S. Wu. 2001. Cell line dependent involvement of ceramide in ultraviolet light-induced apoptosis. *Mol. Cell. Biochem.* **219**: 21–27.
- Dbaibo, G. S., W. El-Assaad, A. Krikorian, B. Liu, K. Diab, N. Z. Idriss, M. El-Sabban, T. A. Driscoll, D. K. Perry, and Y. A. Hannun. 2001. Ceramide generation by two distinct pathways in tumor necrosis factor alpha-induced cell death. *FEBS Lett.* **503**: 7–12.
- Suzuki, J., K. Akahane, J. Nakamura, K. Naruse, H. Kamiya, T. Himeno, N. Nakamura, T. Shibata, M. Kondo, H. Nagasaki, et al. 2011. Palmitate induces apoptosis in Schwann cells via both ceramide-dependent and independent pathways. *Neuroscience.* **176**: 188–198.
- Pettus, B. J., C. E. Chalfant, and Y. A. Hannun. 2002. Ceramide in apoptosis: an overview and current perspectives. *Biochim. Biophys. Acta.* **1585**: 114–125.
- German, O. L., G. E. Miranda, C. E. Abraham, and N. P. Rotstein. 2006. Ceramide is a mediator of apoptosis in retina photoreceptors. *Invest. Ophthalmol. Vis. Sci.* **47**: 1658–1668.
- Sanvicens, N., and T. G. Cotter. 2006. Ceramide is the key mediator of oxidative stress-induced apoptosis in retinal photoreceptor cells. *J. Neurochem.* **98**: 1432–1444.
- Chen, H., A. Y. Chan, D. U. Stone, and N. A. Mandal. 2014. Beyond the cherry-red spot: Ocular manifestations of sphingolipid-mediated neurodegenerative and inflammatory disorders. *Surv. Ophthalmol.* **59**: 64–76.
- Stiles, M., H. Qi, E. Sun, J. Tan, H. Porter, J. Allegood, C. E. Chalfant, D. Yasumura, M. T. Matthes, M. M. LaVail, et al. 2016. Sphingolipid profile alters in retinal dystrophic P23H–1 rats and systemic FTY720 can delay retinal degeneration. *J. Lipid Res.* **57**: 818–831.
- Berdyshev, E. V., I. Gorshkova, A. Skobeleva, R. Bittman, X. Lu, S. M. Dudek, T. Mirzapoiazova, J. G. Garcia, and V. Natarajan. 2009. FTY720 inhibits ceramide synthases and up-regulates dihydrospingosine 1-phosphate formation in human lung endothelial cells. *J. Biol. Chem.* **284**: 5467–5477.
- Lahiri, S., H. Park, E. L. Laviad, X. Lu, R. Bittman, and A. H. Futerman. 2009. Ceramide synthesis is modulated by the sphingosine analog FTY720 via a mixture of uncompetitive and noncompetitive inhibition in an Acyl-CoA chain length-dependent manner. *J. Biol. Chem.* **284**: 16090–16098.
- Olivera, A., and S. Spiegel. 1993. Sphingosine-1-phosphate as second messenger in cell proliferation induced by PDGF and FCS mitogens. *Nature.* **365**: 557–560.
- Hannun, Y. A., and L. M. Obeid. 2008. Principles of bioactive lipid signaling: lessons from sphingolipids. *Nat. Rev. Mol. Cell Biol.* **9**: 139–150.
- Abe, T., H. Tomita, T. Ohashi, K. Yamada, Y. Takeda, K. Akaishi, M. Yoshida, M. Sato, and M. Tamai. 1999. Characterization of iris

- pigment epithelial cell for auto cell transplantation. *Cell Transplant.* **8**: 501–510.
35. Mandal, M. N., J. M. Patlolla, L. Zheng, M. P. Agbaga, J. T. Tran, L. Wicker, A. Kasus-Jacobi, M. H. Elliott, C. V. Rao, and R. E. Anderson. 2009. Curcumin protects retinal cells from light-and oxidant stress-induced cell death. *Free Radic. Biol. Med.* **46**: 672–679.
 36. Qi, H., S. Priyadarshini, S. E. Nicholas, A. Sarker-Nag, J. Allegood, C. E. Chalfant, N. A. Mandal, and D. Karamichos. 2017. Analysis of sphingolipids in human corneal fibroblasts from normal and keratoconus patients. *J. Lipid Res.* **58**: 636–648.
 37. Wijesinghe, D. S., J. C. Allegood, L. B. Gentile, T. E. Fox, M. Kester, and C. E. Chalfant. 2010. Use of high performance liquid chromatography-electrospray ionization-tandem mass spectrometry for the analysis of ceramide-1-phosphate levels. *J. Lipid Res.* **51**: 641–651.
 38. Wijesinghe, D. S., M. Brentnall, J. A. Mietla, L. A. Hoeflerlin, R. F. Diegelmann, L. H. Boise, and C. E. Chalfant. 2014. Ceramide kinase is required for a normal eicosanoid response and the subsequent orderly migration of fibroblasts. *J. Lipid Res.* **55**: 1298–1309.
 39. Chen, H., J. T. Tran, R. E. Anderson, and M. N. Mandal. 2012. Caffeic acid phenethyl ester protects 661W cells from H₂O₂-mediated cell death and enhances electroretinography response in dim-reared albino rats. *Mol. Vis.* **18**: 1325–1338.
 40. Mandal, M. N., and R. Ayyagari. 2006. Complement factor H: spatial and temporal expression and localization in the eye. *Invest. Ophthalmol. Vis. Sci.* **47**: 4091–4097.
 41. Mandal, M. N., G. P. Moiseyev, M. H. Elliott, A. Kasus-Jacobi, X. Li, H. Chen, L. Zheng, O. Nikolaeva, R. A. Floyd, J. X. Ma, et al. 2011. Alpha-phenyl-N-tert-butyl nitron (PBN) prevents light-induced degeneration of the retina by inhibiting RPE65 protein isomerohydrolase activity. *J. Biol. Chem.* **286**: 32491–32501.
 42. Mandal, M. N., V. Vasireddy, M. M. Jablonski, X. Wang, J. R. Heckenlively, B. A. Hughes, G. B. Reddy, and R. Ayyagari. 2006. Spatial and temporal expression of MFRP and its interaction with CTRP5. *Invest. Ophthalmol. Vis. Sci.* **47**: 5514–5521.
 43. Schmittgen, T. D., and K. J. Livak. 2008. Analyzing real-time PCR data by the comparative C(T) method. *Nat. Protoc.* **3**: 1101–1108.
 44. Li, C. M., J. H. Park, X. He, B. Levy, F. Chen, K. Arai, D. A. Adler, C. M. Distche, J. Koch, K. Sandhoff, et al. 1999. The human acid ceramidase gene (ASAH): structure, chromosomal location, mutation analysis, and expression. *Genomics.* **62**: 223–231.
 45. Beatty, S., H. Koh, M. Phil, D. Henson, and M. Boulton. 2000. The role of oxidative stress in the pathogenesis of age-related macular degeneration. *Surv. Ophthalmol.* **45**: 115–134.
 46. Jarrett, S. G., and M. E. Boulton. 2012. Consequences of oxidative stress in age-related macular degeneration. *Mol. Aspects Med.* **33**: 399–417.
 47. Liang, F. Q., and B. F. Godley. 2003. Oxidative stress-induced mitochondrial DNA damage in human retinal pigment epithelial cells: a possible mechanism for RPE aging and age-related macular degeneration. *Exp. Eye Res.* **76**: 397–403.
 48. Kowluru, R. A., and P. S. Chan. 2007. Oxidative stress and diabetic retinopathy. *Exp. Diabetes Res.* **2007**: 43603.
 49. Campochiaro, P. A., R. W. Strauss, L. Lu, G. Hafiz, Y. Wolfson, S. M. Shah, R. Sophie, T. A. Mir, and H. P. Scholl. 2015. Is there excess oxidative stress and damage in eyes of patients with retinitis pigmentosa? *Antioxid. Redox Signal.* **23**: 643–648.
 50. Garanto, A., N. A. Mandal, M. Egidio-Gabas, G. Marfany, G. Fabrias, R. E. Anderson, J. Casas, and R. Gonzalez-Duarte. 2013. Specific sphingolipid content decrease in Cerkl knockdown mouse retinas. *Exp. Eye Res.* **110**: 96–106.
 51. Gómez-Muñoz, A. 2006. Ceramide 1-phosphate/ceramide, a switch between life and death. *Biochim. Biophys. Acta.* **1758**: 2049–2056.
 52. Maceyka, M., S. G. Payne, S. Milstien, and S. Spiegel. 2002. Sphingosine kinase, sphingosine-1-phosphate, and apoptosis. *Biochim. Biophys. Acta.* **1585**: 193–201.
 53. Tani, M., M. Ito, and Y. Igarashi. 2007. Ceramide/sphingosine/sphingosine 1-phosphate metabolism on the cell surface and in the extracellular space. *Cell. Signal.* **19**: 229–237.
 54. Huwiler, A., and J. Pfeilschifter. 2006. Altering the sphingosine-1-phosphate/ceramide balance: a promising approach for tumor therapy. *Curr. Pharm. Des.* **12**: 4625–4635.
 55. Chimin, P., M. L. Andrade, T. Belchior, V. A. Paschoal, J. Magdalon, A. S. Yamashita, E. Castro, A. Castoldi, A. B. Chaves-Filho, M. Y. Yoshinaga, et al. 2017. Adipocyte mTORC1 deficiency promotes adipose tissue inflammation and NLRP3 inflammasome activation via oxidative stress and de novo ceramide synthesis. *J. Lipid Res.* **58**: 1797–1807.
 56. Levy, M., and A. H. Futerman. 2010. Mammalian ceramide synthases. *IUBMB Life.* **62**: 347–356.
 57. Grösch, S., S. Schifffmann, and G. Geisslinger. 2012. Chain length-specific properties of ceramides. *Prog. Lipid Res.* **51**: 50–62.
 58. Süban, J., R. Tidhar, and A. H. Futerman. 2010. Ceramide synthases: roles in cell physiology and signaling. *Adv. Exp. Med. Biol.* **688**: 60–71.
 59. Mullen, T. D., Y. A. Hannun, and L. M. Obeid. 2012. Ceramide synthases at the centre of sphingolipid metabolism and biology. *Biochem. J.* **441**: 789–802.
 60. Kitatani, K., J. Idkowiak-Baldys, and Y. A. Hannun. 2008. The sphingolipid salvage pathway in ceramide metabolism and signaling. *Cell. Signal.* **20**: 1010–1018.
 61. Levade, T., H. W. Moser, A. H. Fensom, K. Harzer, A. B. Moser, and R. Salvayre. 1995. Neurodegenerative course in ceramidase deficiency (Farber disease) correlates with the residual lysosomal ceramide turnover in cultured living patient cells. *J. Neurol. Sci.* **134**: 108–114.
 62. Tan, S. F., X. Liu, T. E. Fox, B. M. Barth, A. Sharma, S. D. Turner, A. Awwad, A. Dewey, K. Doi, B. Spitzer, et al. 2016. Acid ceramidase is upregulated in AML and represents a novel therapeutic target. *Oncotarget.* **7**: 83208–83222.
 63. Hennessy, B. T., D. L. Smith, P. T. Ram, Y. Lu, and G. B. Mills. 2005. Exploiting the PI3K/AKT pathway for cancer drug discovery. *Nat. Rev. Drug Discov.* **4**: 988–1004.
 64. Galadari, S., A. Rahman, S. Pallichankandy, and F. Thayyullathil. 2015. Tumor suppressive functions of ceramide: evidence and mechanisms. *Apoptosis.* **20**: 689–711.
 65. Dumitru, C. A., Y. Zhang, X. Li, and E. Gulbins. 2007. Ceramide: a novel player in reactive oxygen species-induced signaling? *Antioxid. Redox Signal.* **9**: 1535–1540.
 66. Takeda, Y., M. Tashima, A. Takahashi, T. Uchiyama, and T. Okazaki. 1999. Ceramide generation in nitric oxide-induced apoptosis. Activation of magnesium-dependent neutral sphingomyelinase via caspase-3. *J. Biol. Chem.* **274**: 10654–10660.
 67. Wu, B. X., Y. H. Zeidan, and Y. A. Hannun. 2009. Downregulation of neutral ceramidase by gemcitabine: Implications for cell cycle regulation. *Biochim. Biophys. Acta.* **1791**: 730–739.
 68. Rath, G., C. Schneider, B. Langlois, H. Sartelet, H. Morjani, H. E. Btaouri, S. Dedieu, and L. Martiny. 2009. De novo ceramide synthesis is responsible for the anti-tumor properties of camptothecin and doxorubicin in follicular thyroid carcinoma. *Int. J. Biochem. Cell Biol.* **41**: 1165–1172.
 69. Dbaibo, G. S., Y. Kfoury, N. Darwiche, S. Panjarian, L. Kozhaya, R. Nasr, M. Abdallah, O. Hermine, M. El-Sabban, H. de The, et al. 2007. Arsenic trioxide induces accumulation of cytotoxic levels of ceramide in acute promyelocytic leukemia and adult T-cell leukemia/lymphoma cells through de novo ceramide synthesis and inhibition of glucosylceramide synthase activity. *Haematologica.* **92**: 753–762.
 70. Kizhakkayil, J., F. Thayyullathil, S. Chathoth, A. Hago, M. Patel, and S. Galadari. 2012. Glutathione regulates caspase-dependent ceramide production and curcumin-induced apoptosis in human leukemic cells. *Free Radic. Biol. Med.* **52**: 1854–1864.
 71. Manning, B. D., and L. C. Cantley. 2007. AKT/PKB signaling: navigating downstream. *Cell.* **129**: 1261–1274.
 72. Thayyullathil, F., S. Chathoth, A. Shahin, J. Kizhakkayil, A. Hago, M. Patel, and S. Galadari. 2011. Protein phosphatase 1-dependent dephosphorylation of Akt is the prime signaling event in sphingosine-induced apoptosis in Jurkat cells. *J. Cell. Biochem.* **112**: 1138–1153.
 73. Chalfant, C. E., K. Kishikawa, M. C. Mumby, C. Kamibayashi, A. Bielawska, and Y. A. Hannun. 1999. Long chain ceramides activate protein phosphatase-1 and protein phosphatase-2A. Activation is stereospecific and regulated by phosphatidic acid. *J. Biol. Chem.* **274**: 20313–20317.
 74. Wolff, R. A., R. T. Dobrowsky, A. Bielawska, L. M. Obeid, and Y. A. Hannun. 1994. Role of ceramide-activated protein phosphatase in ceramide-mediated signal transduction. *J. Biol. Chem.* **269**: 19605–19609.
 75. Salinas, M., R. Lopez-Valdaliso, D. Martin, A. Alvarez, and A. Cuadrado. 2000. Inhibition of PKB/Akt1 by C2-ceramide involves activation of ceramide-activated protein phosphatase in PC12 cells. *Mol. Cell. Neurosci.* **15**: 156–169.
 76. Schubert, K. M., M. P. Scheid, and V. Duronio. 2000. Ceramide inhibits protein kinase B/Akt by promoting dephosphorylation of serine 473. *J. Biol. Chem.* **275**: 13330–13335.

77. Czubowicz, K., and R. Strosznajder. 2014. Ceramide in the molecular mechanisms of neuronal cell death. The role of sphingosine-1-phosphate. *Mol. Neurobiol.* **50**: 26–37.
78. Remé, C. E., C. Grimm, F. Hafezi, A. Marti, and A. Wenzel. 1998. Apoptotic cell death in retinal degenerations. *Prog. Retin. Eye Res.* **17**: 443–464.
79. Czabotar, P. E., G. Lessene, A. Strasser, and J. M. Adams. 2014. Control of apoptosis by the BCL-2 protein family: implications for physiology and therapy. *Nat. Rev. Mol. Cell Biol.* **15**: 49–63.
80. Feng, C., X. Wang, T. Liu, M. Zhang, G. Xu, and Y. Ni. 2017. Expression of CCL2 and its receptor in activation and migration of microglia and monocytes induced by photoreceptor apoptosis. *Mol. Vis.* **23**: 765–777.
81. Satoh, S., A. K. Nussler, Z. Z. Liu, and A. W. Thomson. 1994. Proinflammatory cytokines and endotoxin stimulate ICAM-1 gene expression and secretion by normal human hepatocytes. *Immunology.* **82**: 571–576.
82. Foresti, R., S. K. Bains, T. S. Pitchumony, L. E. de Castro Bras, F. Drago, J. L. Dubois-Rande, C. Bucolo, and R. Motterlini. 2013. Small molecule activators of the Nrf2-HO-1 antioxidant axis modulate heme metabolism and inflammation in BV2 microglia cells. *Pharmacol. Res.* **76**: 132–148.
83. Myśliwiec, M., A. Balcerska, K. Zorena, J. Myśliwska, P. Lipowski, and K. Raczyńska. 2008. The role of vascular endothelial growth factor, tumor necrosis factor alpha and interleukin-6 in pathogenesis of diabetic retinopathy. *Diabetes Res. Clin. Pract.* **79**: 141–146.
84. Yao, J., H. E. Bi, Y. Sheng, L. B. Cheng, R. L. Wendu, C. H. Wang, G. F. Cao, and Q. Jiang. 2013. Ultraviolet (UV) and hydrogen peroxide activate ceramide-ER stress-AMPK signaling axis to promote retinal pigment epithelium (RPE) cell apoptosis. *Int. J. Mol. Sci.* **14**: 10355–10368.
85. Acharya, U., S. Patel, E. Koundakjian, K. Nagashima, X. Han, and J. K. Acharya. 2003. Modulating sphingolipid biosynthetic pathway rescues photoreceptor degeneration. *Science.* **299**: 1740–1743.